Sánchez Diana, LD.; Olivares-Sánchez-Mellado, I.; Parra Gómez, J.; Menghini, M.; Homm, P.; Locquet, J.; Sanchis Kilders, P. (01-0). Experimental demonstration of a tunable transverse electric pass polarizer based on hybrid VO2/silicon technology. Optics Letters. 43(15):3650-3653. https://doi.org/10.1364/OL.43.003650

Experimental demonstration of a tunable transverse electric pass polarizer based on hybrid VO_2/silicon technology

Luis David Sánchez[1], Irene Olivares[1], Jorge Parra[1], Mariela Menghini[2], Pía Homm[2], Jean-Pierre Locquet[2], Pablo Sanchis[1,*]

[1] *Nanophotonics Technology Center, Universitat Politècnica de València, Camino de Vera s/n, 46022 Valencia, Spain*
[2] *Department of Physics and Astronomy, KU Leuven, Celestijnenlaan 200D, Leuven, Belgium*
**Corresponding author: pabsanki@ntc.upv.es*

Received XX Month XXXX; revisedXX Month, XXXX; accepted XX MonthXXXX; posted XX Month XXXX (Doc. ID XXXXX); published XX Month XXXX

A tunable transverse electric (TE) pass polarizer is demonstrated based on hybrid VO_2/Si (vanadium dioxide/silicon) technology. The 20 μm-long TE pass polarizer exploits the phase transition of the active VO_2 material to control the rejection of the unwanted transverse magnetic (TM) polarization. Characterized for the wavelength range from 1540 nm to 1570 nm, the device features insertion losses below 1 dB at static conditions and insertion losses of 5 dB and an attenuation of TM polarization of 19 dB in the active state. To the best of our knowledge, this is the first time that tunable polarizers compatible with silicon photonics are demonstrated. © 2018 Optical Society of America

OCIS codes: *(230.7370) Waveguides; (250.5300) Photonic Integrated Circuits; (130.5440) Polarization-selective devices*

http://dx.doi.org/10.1364/OL.99.099999

Silicon waveguides show a high polarization dependence due to the high index contrast and birefringence. Therefore, a key feature to ensure optimum performance of silicon photonic chips is polarization management. Several polarization management devices, like polarizers or rotators, have been proposed in the silicon-on-insulator (SOI) platform [1-7] or using the plasmonic technology [8-14]. Compact devices have been demonstrated with plasmonics but at the cost of high insertion losses due to the interaction between light and metals. In contrast, highly efficient and low loss devices have been demonstrated based on silicon but normally with large footprints. However, polarization tunability remains still as an open challenge. Hybrid technologies based on the combination of the SOI platform with tunable materials are a promising route. Recently, phase transition materials such as correlated functional oxides have been proposed for the development of tunable photonic devices [15-24]. These materials are characterized by a reversible phase transition controlled by an external stimulus, which induces a relevant change in the optical and electrical properties of the material. Among them, vanadium dioxide (VO_2) has acquired a significant status.

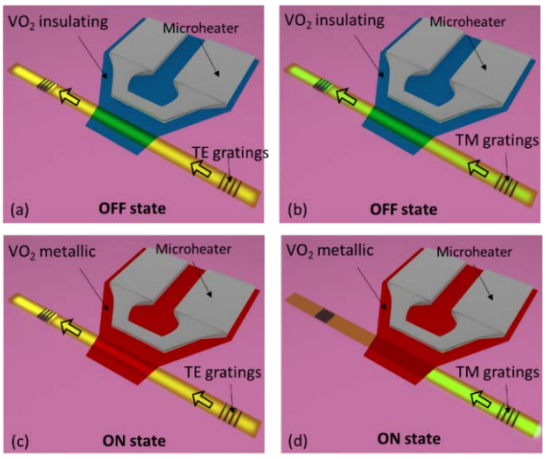

Fig. 1. Concept art of the proposed TE pass polarizer as a function of the input polarization and VO_2 states. On one hand, for VO_2 in the insulating state (OFF state), both (a) TE and (b) TM polarizations go through the polarizer with low losses. On the other hand, for VO_2 in the metallic state (ON state), the polarizer introduces low losses for (c) TE polarization and high losses for (d) TM polarization. The state in VO_2 is changed via Joule heat induced by a lateral microheater.

By applying a thermal [25-27], electrical [28-34] or optical [35, 36] excitation, VO_2 goes through a reversible transition from an insulating state at steady conditions to a metallic state under the influence of the external signal. The phase transition provides an ultra-large change in the imaginary part of the refractive index allowing to tune the material from a state with low losses to a state with high losses. Such optical loss variation could be exploited to

control light polarization by integrating the VO_2 into a polarization-dependent waveguide structure. Therefore, the combination of a passive polarizer structure with the effect of the phase transition in VO_2 may provide tunability over the rejection of the unwanted polarization. The on-chip combination of the proposed tunable pass polarizer with other components, such as polarization splitters, could open new ways of manipulating the polarization of light in silicon devices with potential applications in different fields such as data communications, instrumentation or sensors.

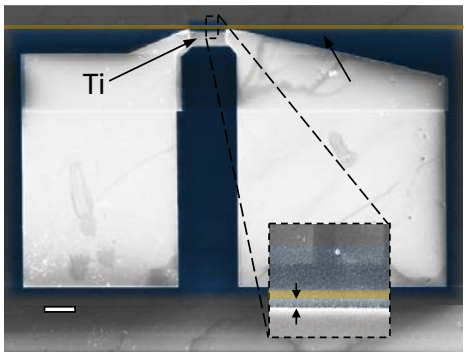

Fig. 2. SEM image of the fabricate device showing the silicon waveguide and the lateral microheater with the double Ti-AlCu metallization. The inset shows a zoom over the hybrid VO2/Si area where the granular texture of the VO2 layer can be observed. False colours have been used to highlight the silicon waveguide and the VO_2 layer.

In this work, we demonstrate a tunable transverse electric (TE) pass polarizer based on a hybrid VO_2/Si waveguide. The performance of the polarizer is based on the fact that the interaction between the optical mode and a VO_2 thin film deposited on top of a silicon waveguide is different depending on the polarization. Thus, the control over the transverse magnetic (TM) polarization is achieved by taking advantage of the refractive index change in VO_2 across its insulating to metal transition. To the best of our knowledge, this is the first time that tunable polarizers compatible with silicon photonics are experimentally demonstrated. The device exhibits a compact footprint with a total length of only 20 μm, insertion losses ranging from 1 dB to 5.5 dB, attenuation of the TM polarization above 19 dB and broadband operation.

Figure 1 shows concept arts of the proposed tunable TE pass polarizer for both states in VO_2 when the input mode has different polarization. On one hand, for the insulating state (OFF state), Figs. 1 (a)–(b), the light travels through the polarizer with low losses independently of the polarization. On the other hand, for the metallic state (ON state), the VO_2 has a low influence on the TE polarization, Fig. 1(c), but introduces high optical losses for TM polarization, Fig. 1(d). Therefore, by changing the state in VO_2 it is possible to control the attenuation of TM polarization. The hybrid VO_2/Si waveguide is composed by a granular VO_2 thin film of around 15 nm in thickness and a single-mode silicon waveguide with a cross section of 480 nm x 220 nm. The silicon waveguide is separated from the active VO_2 layer by a 60 nm-thick layer made of 50 nm-thick nitride on top of 10 nm-thick silica. The nitride layer is needed for the chemical mechanical planarization (CMP) process. The phase transition in VO_2 is controlled via Joule heating induced by a lateral microheater displaced 550 nm from the hybrid waveguide, as shown in Fig. 1. When an electrical current is flowing through the microheater, the generated heat is focused onto the hybrid VO_2/Si waveguide inducing the metallic state in VO_2.

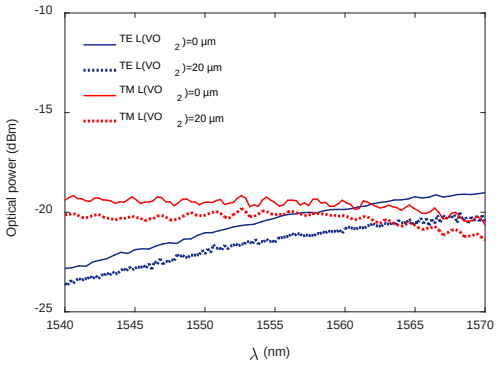

Fig. 3. Measured transmission spectra of the devices with and without the 20 μm-long VO_2 layer for both polarizations. VO2 layer in static conditions.

Two identical hybrid VO_2/Si waveguide structures but with different grating couplers for TE or TM polarization, as depicted in Fig. 1, have been fabricated to characterize the device performance. The fabrication of the VO_2 layer has been carried out by molecular beam epitaxy (MBE) followed by an ex-situ annealing process [37]. We have recently demonstrated that the insertion losses of the device can be minimized by using a VO_2 layer with a granular morphology [38]. The granular morphology was the result of an additional solvent bath step during the exposure/lift-off processes. Figure 2 displays shows a SEM images of the fabricated device with granular VO_2. The microheater is based on a double metallization of titanium (Ti) and aluminium-copper (AlCu) as depicted in Fig. 2. The Ti section has a width of 7 μm. Ti has a much higher resistivity than AlCu so the heat is concentrated in this section, which contributes to minimize the power consumption [39].

The insertion losses of the device in passive conditions, VO_2 layer in the static state, have been firstly characterized. Figure 3 shows the measured transmission spectra of the devices with and without the 20 μm-long hybrid VO_2/Si waveguide section for both polarizations. The observed wavelength dependence is determined by the slightly different grating response for each polarization. Insertion losses below 1 dB and a broadband operation (> 30nm) are achieved for both TE and TM polarizations. Once the passive performance of the device has been characterized, the phase transition in VO_2 to the metallic state has been measured by applying different electrical power levels to the microheater.

Figure 4 shows, for an input wavelength of 1550 nm, the optical losses for TE and TM polarizations as a function of increasing and decreasing electrical power sweeps. A hysteretic response inherent to the phase transition in VO_2 is observed independently of the polarization. An electrical power of around 70 mW is sufficient to have the maximum attenuation of 19 dB for TM polarization. The power consumption may be reduced by reducing the lateral displacement between the microheater and the silicon. Another approach to reduce the power consumption could be to decrease the VO_2 phase transition temperature to a value closer to room temperature. It has been shown that the transition temperature can be reduced and the width of the hysteresis can be modified (or even suppressed) by using different dopant elements [40-42].

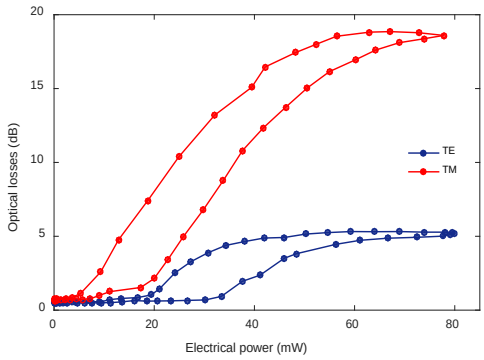

Fig. 4. Optical losses for TE and TM polarizations as a function of the applied electrical power to the microheater for the proposed TE pass polarizer.

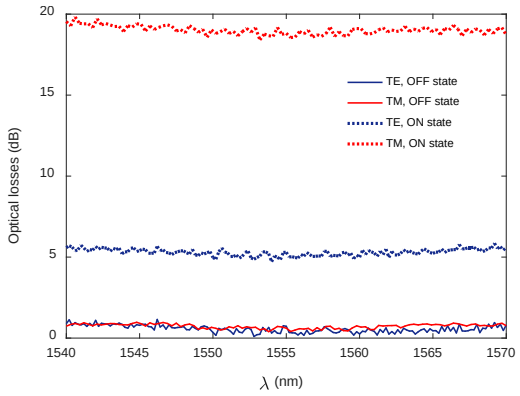

Fig. 5. Optical losses as a function of the wavelength of the proposed TE polarizer depending on the input polarization and the state in the VO_2 active layer. The ON state has been achieved by applying an electrical power of 70 mW to the microheater.

Figure 5 shows the optical losses as a function of the wavelength of the proposed TE polarizer depending on the input polarization and the state in the VO_2 active layer. The broadband performance of the device is confirmed. On one hand, in static conditions of VO_2 (OFF state), insertion losses are below 1 dB for both polarizations. On the other hand, when an electrical power of 70 mW is applied to the device (ON state), the insertion losses for TE polarization increase to around 5 dB while the TM polarization is highly attenuated with optical losses around 19 dB.

Low insertion losses in the device have been achieved due to the granular morphology of the VO_2 layer. Simulations have been carried out to analyze the influence of such morphology on the device performance. The effect of the granularity has been modelled by the Maxwell-Garnett effective-medium theory (EMT) [43]. Maxwell-Garnett EMT has been proved to describe the effective permittivity of inhomogeneous VO_2 thin films [44]. Therefore, the variation of optical losses has been simulated for the hybrid VO_2/Si waveguide by considering a 15 nm-thick VO_2 layer with an effective refractive index dependent on the volume fraction occupied by the VO_2 in air.

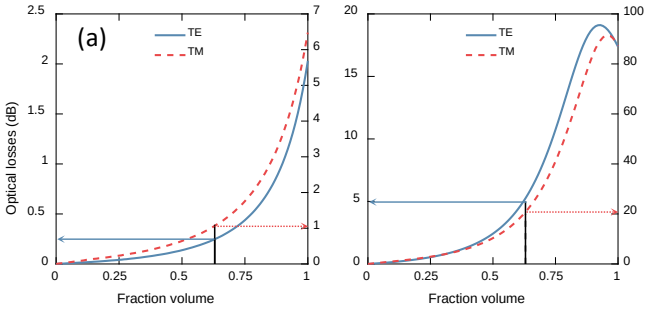

Fig. 6. Simulated optical losses of the hybrid VO2/Si waveguide as a function of the fraction volume (f) occupied by the VO2 in air. Values have been calculated for TE and TM polarizations taking into account a 15 nm-thick VO2 film in the (a) insulating and (b) metallic states with effective refractive indices calculated by using the Maxwell-Garnett EMT.

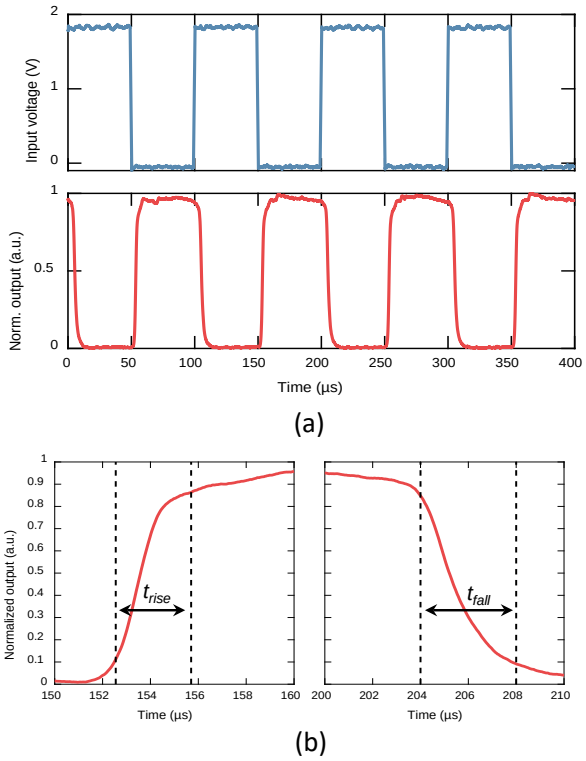

Fig. 7. (a) Electrical driving signal applied to the microheater and photodetected signal at the output of the polarizer for TM polarization. (b) Zoom of the photodetected output signal showing the rise and fall times.

Results are shown in Fig. 6 for the effective VO_2 layer in the (a) insulating and (b) metallic states. Refractive index values of $3.21+0.17i$ and $2.15+2.79i$ for VO_2 in the insulating and metallic states, respectively, have been taken from the literature [16]. Simulated optical losses for both TE and TM polarizations and VO_2 in the insulating and metallic states are in very good agreement with the experimental values shown in Fig. 5 for a fraction volume around 0.65. The fraction volume of VO_2 was also estimated from a

binarized crop of the SEM image to discriminate the VO_2 particles. From this technique, $f = 0.66 \pm 0.07$ was obtained, which is also in very good agreement with the value derived from simulations.

The temporal response of the polarizer was characterized by applying a square signal of 10 kHz with a 50% duty cycle to the microheater. Figure 7(a) shows the electrical driving signal and the photodetected signal at the output of the polarizer for TM polarization. On one hand, when voltage is applied to the microheater, the output signal is highly attenuated due to the VO_2 change from insulating to metallic state. On the other hand, when the applied voltage is released, the VO_2 returns to the insulating state and therefore to the low-loss state. The speed of the device can be obtained from the rise and fall times (see Fig. 7b), which are 3.16 and 3.91 μs, respectively. The small differences between rise and fall times can be explained from the hysteretic response of the VO_2 and the non-linear temperature change with time of the heating-up and cooling-down processes [45].

In conclusion, a tunable hybrid VO_2/silicon TE pass polarizer has been demonstrated. The rejection of the unwanted polarization is controlled by tuning the optical losses across the phase transition in the VO_2 active material. A granulated morphology of the VO_2 film allowed to reduce insertion losses while keeping a high polarization extinction ratio. Therefore, texturized VO_2 films could be exploited as an efficient mechanism to improve the performance of novel active devices based on VO_2/Si technology.

Funding. TEC2016-76849 (MINECO/FEDER, UE) and H2020-PHRESCO (688579) projects.

Acknowledgment. SOI samples were fabricated at IHP (we acknowledge Lars Zimmermann) in the framework of SITOGA project. I. O. acknowledges the Universitat Politècnica de València for funding her grant. P.H. acknowledges support from Becas Chile-CONICYT.

REFERENCES

1. L. Liu, Y. Ding, K. Yvind, and J. M. Hvam, Opt. Lett. **36**, 1059 (2011).
2. C. Alonso-Ramos, R. Halir, A. Ortega-Moñux, P. Cheben, L. Vivien, I. Molina-Fernández, D. Marris-Morini, S. Janz, D.-X. Xu, and J. Schmid, Opt. Lett. **37**, 3534 (2012)
3. H. Zhang, S. Das, J. Zhang, Y. Huang, C. Li, S. Chen and J. T. Thong, Appl. Phys. Lett, **101**, 021105 (2012).
4. S. I. Azzam, M. F. Hameed, N F. Areed, M. M. Abd-Elrazzak, H. A. El-Mikaty and S. S. Obayya, IEEE Photon. Technol. Lett., **26**, 1633 (2014).
5. D. Dai, Z. Wang, N. Julian and J. E. Bowers, Opt. Express **18**, 27404 (2010).
6. M. Aamer, A. M. Gutierrez, A. Brimont, D. Vermeulen, G. Roelkens, J. M. Fedeli, A. Hakansson and P. Sanchis, IEEE Photon. Technol. Lett., **24**, 2031 (2012).
7. Y. Xiong, D.-X. Xu, J. H. Schmid, P. Cheben, W. N. Ye, IEEE Photon. J., **7**, 1 (2015).
8. L. Sánchez and P. Sanchis, Opt. Lett. **38**, 2842 (2013).
9. M. A. Komatsu, K. Saitoh, and M. Koshiba, IEEE Photon. J., **4**, 707 (2012).
10. N. Caspers, M. Z. Alam, and M. Mojahedi, Opt. Lett. **37**, 4615 (2012).
11. X. Sun, M. Z. Alam, S. J. Wagner, J. S. Aitchison, and M. Mojahedi, Opt. Lett. **37**, 4814 (2012).
12. M. Z. Alam, J. S. Aitchison, and M. Mojahedi, Opt. Lett. **37**, 55 (2012).
13. L. Jin, Q. Chen, and L. Wen, Opt. Lett. **39**, 2798 (2014).
14. J. N. Caspers, J. S. Aitchison, and M. Mojahedi, Opt. Lett. **38**, 4054 (2013).
15. Z. Yang, and S. Ramanathan, IEEE Photon J., **7**, 0700305 (2015).
16. R. M. Briggs, I. M. Pryce, and H. A. Atwater, Opt. Express **18**, 11192 (2010).
17. J. D. Ryckman, K. A. Hallman, R. E. Marvel, R. F. Haglund, and S. M. Weiss, Opt. Express **21**, 10753 (2013).
18. P. Markov, R. E. Marvel, H. J. Conley, K. J. Miller, R. F. Haglund, Jr., and S. M. Weiss, ACS Photonics **2**, 1175 (2015).
19. A. Joushaghani, J. Jeong, S. Paradis, D. Alain, J. S. Aitchison and J. K. S. Poon, Opt. Expr. **23**, 3657 (2015).
20. L. Sanchez, S. Lechago and P. Sanchis, Opt. letters, **40**, 1452 (2015).
21. L. Sanchez, S. Lechago, A. Gutierrez and P. Sanchis, IEEE Phot. Journal, **8**, 1 (2016).
22. M. Sun, W. Shieh and R.R. Unnithan, IEEE Phot. Journal, **9**, 1 (2017).
23. K. J. Miller, K. A. Hallman, R. F. Haglund, and S. M. Weiss, Opt. Express, 25, 26527 (2017).
24. J.K.Clark, Y.L.Ho, H.Matsui and J.J.Delaunay, IEEE Phot. Journal, **10**, 1 (2018).
25. C. Ko and S. Ramanathan, App. Phys. Lett., **93**, 1 (2008).
26. A.Zimmers, L.Aigouy, M.Mortier, A.Sharoni, S.Wang, K.West, J.Ramirez, and I.Schuller, Phys. Rev. Lett. **110**, 1 (2013).
27. M.A.Kats, R.Blanchard, P.Genevet, Z.Yang, M.M.Qazilbash, D.N.Basov, S.Ramanathan and F.Capasso, Opt. Lett., **38**, 368 (2013).
28. B.G.Chae, H.T.Kim, D.H.Youn and K.Y.Kang, Phys. B Condens. Matter, **369**, 76 (2005).
29. D.Ruzmetov, G.Gopalakrishnan, J.Deng, V.Narayanamurti and S.Ramanathan,J.Appl.Phys. **106**, 1 (2009).
30. S. B.Lee, K.Kim, J.S.Oh, B.Kahng and J.S.Lee, Appl. Phys. Lett., **102**, 1 (2013).
31. A.Joushaghani, J.Jeong, S.Paradis, D.Alain, J.S. Aitchison and J.K.S.Poon, Appl. Phys. Lett. **104**, 1 (2014).
32. Z.Yang, S.Hart, C.Ko, A.Yacoby and S.Ramanathan, Journ. of App.Phys. **110**, 033725 (2011)
33. J. Yoon, G. Lee, C.Park, B.S.Mun and H.Ju, App. Phys. Lett. **105**, 083503 (2014).
34. L. Sanchez, A. Rosa, A. Griol, A. Gutierrez, P. Homm, B. Van Bilzen, M. Menghini, J. P. Locquet, and P. Sanchis, Appl. Phys. Lett. **111,** 31904 (2017).
35. J. D.Ryckman. V.D.Blanco, J.Nag, R.E.Marvel, B. K. Choi, R. F. Haglund and S. M. Weiss, Opt. Expr. **20**, 13215 (2012).
36. E. Abreu, S. N. Gilbert Corder, S. Jin Yun, S. Wang, J. G. Ramírez, K. West, J. Zhang, S. Kittiwatanakul, I. K. Schuller, J. Lu, S. A. Wolf, H.-T. Kim, M. Liu, and R. D. Averitt, Phys. Rev. B **96**, 094309 (2017).
37. B. Van Bilzen, P. Homm, L. Dillemans, C.-Y Su, M. Menghini, M. Sousa, C. Marchiori, L. Zhang, J. W. Seo and J.-P. Locquet, Thin Solid Films **591**, 143 (2015).
38. I. Olivares, L. Sanchez, J. Parra, R. Larrea, A. Griol, M. Menghini, P. Homm, L.-W. Jang, B. Van Bilzen, J.W. Seo, J.-P. Locquet, and P. Sanchis, Opt. Express **26**, 12387 (2018).
39. A. Rosa, A. Gutierrez, A. Brimont, A. Griol, and P. Sanchis, Opt. Express **24**, 191-198 (2016).
40. K. Shibuya, M. Kawasaki and Y. Tokura, Appl. Phys. Lett. **96**, 022102 (2010).
41. S. Hu, S. –Y. Li, R. Ahuja, C. G. Granqvist, K. Hermansson, G. A. Niklasson and R. H. Scheicher, Appl. Phys. Lett. **101**, 201902 (2012).
42. K. Miyazaki, K. Shibuya, M. Suzuki, H. Wado and A. Sawa, Jap. Jour. Appl. Phys**. 53**, 071102 (2014).
43. G. A. Niklasson, Granqvist, C. G. Granqvist and O. Hundrei, *Appl. Opt.*, **20**(1)**,** 26-30 (1981).
44. P. U. Jepsen, B. M. Fischer, A. Thomas, H. Helm, J. Y. Suh, R. López and R. F. Haglund, Jr., *Phys. Rev. B*, **74,** 205103 (2006).
45. X. Fang and L. Yang, *J. Semicond.*, **38,** 104004 (2017).